Priority-guided Search Strategy and Cyber-Physical Energy System Design for Industrial Sericulture

Wen-Bin Zhao[a,c], Jun-Han Hu[b], Gao-An Zheng[a,d,*]

[a] *School of Mechanical Engineering, Zhejiang University of Water Resources and Electric Power, Hangzhou, 310018, China*
[b] *College of Mechanical Engineering, Zhejiang University of Technology, Hangzhou, 310023, China*
[c] *Zhejiang Key Laboratory of Pumps and Turbines, Zhejiang University of Water Resources and Electric Power, Hangzhou, 310018, China*
[d] *Zhejiang Engineering Research Center of Advanced Water Conservancy Equipment, Zhejiang University of Water Resources and Electric Power, Hangzhou, 310018, China*

Abstract

Industrial sericulture workshops require reliable temperature–humidity regulation under varying weather conditions, time-of-use electricity prices, and process-induced thermal–humidity loads. To address this control problem, this study formulates a discrete-time optimization model with a 15-min control interval and evaluates it within a Cyber-Physical Energy System (CPES) framework using an EnergyPlus-based co-simulation environment. The control strategy is implemented in a rolling-horizon model predictive control (MPC) manner and incorporates a priority-guided local refinement strategy. The proposed enhancement module (EM) acts as a local refinement layer for baseline heuristic solvers. Baseline heuristic algorithms are first used to generate candidate control sequences, after which EM identifies high-priority time steps based on boundary proximity, electricity price, process load, and action variation and performs restricted local refinement around these steps. Time-step screening, candidate ranking, and pruning are used to reduce the resulting search space. For a fair comparison, heuristic hyperparameters are calibrated on six tuning scenarios, and all methods are subsequently evaluated on eighteen formal scenarios. The EM-enhanced methods reduce the average composite objective by 31.04%–59.56% relative to their baseline

*Corresponding author.
Email address: zhengga@zuwe.edu.cn (Gao-An Zheng)

counterparts. Among the ten main baseline and EM-enhanced methods, EM-enhanced particle swarm optimization (EM-PSO) achieves the lowest average composite objective value of 514.94 and a comfort satisfaction rate of 1.0000. Its advantage over tabu search (TS), simulated annealing (SA), genetic algorithm (GA), and standard particle swarm optimization (PSO) is statistically significant according to the Wilcoxon signed-rank test ($p < 0.01$). An engineering assessment based on enterprise-provided parameters further indicates an approximate 10.92% reduction in total energy consumption under the specified assumptions. These results provide a reproducible framework for control pre-evaluation and establish a basis for subsequent field validation.

Keywords: Cyber-Physical Energy System (CPES), industrial sericulture, EnergyPlus co-simulation, energy optimization, heuristic algorithms, priority-guided local search, model predictive control

---

1. Introduction and Related Work

Industrial sericulture workshops require tight temperature–humidity regulation. Indoor operating conditions and control decisions are affected by weather, time-of-use electricity prices, and process-induced thermal–humidity loads. Inadequate regulation increases operating costs and may compromise production stability. Although rule-based strategies are straightforward to implement, their adaptability to disturbances is limited. Conventional heuristic algorithms can generate feasible control sequences, but they do not necessarily refine the few time steps that dominate comfort and energy performance.

EnergyPlus co-simulation and a Cyber-Physical Energy System (CPES) framework offer a suitable basis for studying this type of closed-loop energy-control problem. EnergyPlus captures the coupled effects of the building envelope, equipment operation, and indoor thermal–humidity response. CPES links sensing, simulation, and optimization in a closed loop. Accordingly, this study focuses on control modeling and optimization rather than communication protocols or hardware architecture.

Three streams of research are particularly relevant to this study: CPES and digital twins, EnergyPlus-based co-simulation, and optimization-based environmental control. Cyber-physical systems and digital twins have been widely applied in manufacturing and facility control [1]. Representative architectural and implementation studies include [2]. Related system-level

digital-twin architectures have also been reported in [3] and [4]. EnergyPlus co-simulation has become increasingly common in protected agriculture [5]. Additional agricultural co-simulation applications are reported in [6]. Greenhouse control studies now cover stochastic predictive control [7], constrained optimization [8], and thermal–humidity forecasting [9]. In parallel, building energy research has developed mature model predictive control (MPC) methods for humidity-aware control [10], event-triggered scheduling [11], thermal comfort management [12], and multi-objective optimization [13]. However, discrete environmental control for industrial sericulture still lacks a concise and reproducible framework that jointly addresses comfort satisfaction, energy cost, and switching behavior under simultaneous electricity-price and process-load fluctuations.

To address this gap, this paper develops a CPES-based EnergyPlus co-simulation framework and a discrete-time optimization model with a 15-min control interval. Baseline heuristic solvers first produce candidate control sequences, after which the proposed priority-guided strategy concentrates local refinement on the identified high-priority time steps. To avoid bias caused by inconsistent parameter settings, all heuristic solvers are calibrated on independent tuning scenarios before formal comparative evaluation.

The main contributions are as follows. (1) A discrete-time optimization model is formulated for temperature–humidity control in industrial sericulture. The model integrates indoor states, external disturbances, equipment actions, energy cost, comfort penalties, and switching penalties. (2) A priority-guided local refinement strategy is developed for rolling-horizon control. It identifies high-priority time steps and refines their actions using two restricted-neighborhood modes, RIGID and FLEX, together with time-step screening, candidate ranking, and pruning. (3) A reproducible scenario set is established in the CPES and EnergyPlus co-simulation environment for separated tuning and formal evaluation. (4) Multi-algorithm comparisons, ablation analysis, runtime evaluation, and an industry-parameter-based case study are conducted to assess the practical value and limitations of the proposed framework.

To clarify how the proposed framework is positioned, the following subsections review the four methodological bases that support the study: CPES and digital-twin concepts, temperature–humidity energy optimization, heuristic search methods, and simulation-based evaluation. These subsections do not introduce separate research objectives; rather, they explain why the proposed closed-loop control framework combines sensing, co-simulation, optimization,

and reproducible scenario testing.

1.1. CPES and Digital Twin Methods

Cyber-Physical Systems (CPS) have increasingly been extended to CPES in applications that couple energy flows, environmental constraints, and production operations. In industrial sericulture, temperature–humidity control, equipment scheduling, and energy use are tightly linked. A CPES framework is therefore well suited for integrating field sensing, co-simulation, and optimization.

Prior studies have established the conceptual basis of digital twins and their industrial implementations [1]. Industrial interpretations and design principles are discussed in [14], [15], and [16]. In industrial Internet of Things settings, CPS provides the system-level control architecture [17], whereas digital twins provide high-fidelity virtual representations for monitoring, prediction, and optimization [18]. A cyber-physical production perspective related to this transition is also described in [19]. The two concepts are closely related but differ in emphasis: CPES highlights closed-loop coordination among sensing, energy, and control modules, whereas digital twins emphasize consistent mapping between physical and virtual systems.

Research on agricultural facilities has progressively moved from conceptual architectures to executable control platforms. Digital twin frameworks have been reported for greenhouse management [5]. Related agricultural industrial-park applications are described in [20]. Comparative studies have highlighted the need to balance model fidelity, online speed, and deployability [21]. Recent greenhouse control studies further indicate a clear trend toward integrating predictive models with optimization-based climate control. This trend motivates the CPES-oriented framework developed in this study for industrial sericulture.

1.2. Energy Optimization in Temperature and Humidity Control

In agricultural facilities and industrial breeding systems, energy optimization is constrained not only by equipment characteristics but also by weather, electricity prices, process-induced thermal–humidity loads, and comfort requirements. This work therefore combines enterprise-provided parameters, simulation models, public meteorological data, and electricity price data to evaluate the controller under unified scenario-driven test cases.

Energy optimization has been widely studied through machine learning [22], multi-objective optimization [23], robust scheduling [24], and CPS-based

monitoring frameworks [25]. Additional multi-energy scheduling examples are reported in [26] and [27]. Recent work in agricultural and livestock systems also points toward low-carbon operation [28] and intelligent cross-system scheduling [29]. In the building domain, MPC studies have matured in humidity control [10], ventilation regulation [30], and energy-efficient supervisory control [31]. Related field-oriented building studies are also reported in [32]. These advances motivate the adaptation of rolling-horizon and priority-guided optimization ideas to industrial sericulture.

1.3. Heuristic Optimization Methods

Heuristic algorithms search for near-optimal feasible solutions through stochastic exploration, rule-based adjustment, or population-based collaboration. Because they do not require convexity or smooth differentiability, they are well suited to nonlinear, discrete, and disturbance-sensitive energy control problems. Such methods have been widely used in building energy optimization, microgrid scheduling, equipment operation planning, and industrial energy conservation.

Different heuristic algorithms are suitable for different types of search landscapes. Classic formulations include simulated annealing [33], tabu search [34], and particle swarm optimization [35]. Later extensions and applications continue to refine these search families [36]. Related PSO-based optimization studies are also reported in [37]. In this study, the baseline set spans a rule-based strategy (RB), tabu search (TS), simulated annealing (SA), a genetic algorithm (GA), and particle swarm optimization (PSO). This range provides a compact comparison basis across different search mechanisms without privileging any single heuristic family in advance.

1.4. Co-Simulation Fundamentals and Research Perspective of This Work

In this study, modeling and simulation (M&S) provides the methodological basis for reproducible pre-deployment evaluation. Modeling defines the variables and constraints of the control problem, whereas simulation provides a repeatable environment for evaluation when physical testing is costly or impractical [38]. Since their early development [39], M&S methods have become standard tools in many engineering domains. Related execution-oriented simulation environments are discussed in [40] and [41].

Model credibility is therefore relevant to the interpretation of the results and is commonly discussed within verification, validation, and accreditation (VV&A) frameworks [42]. Additional guidance is provided by [43] and

[44]. For building and facility energy systems, EnergyPlus co-simulation is especially useful because it couples thermal dynamics, control actions, and external disturbances in an executable environment [6]. Related simulation-platform comparisons are reported in [21]. Within this simulation-based setting, the study focuses on two issues: how to formulate rolling temperature–humidity control with electricity prices and process loads in a CPES setting, and how to improve baseline heuristic solutions through a priority-guided local refinement strategy within the same closed-loop simulation framework.

2. Problem Formulation

This section translates the industrial sericulture control problem into a discrete-time rolling optimization formulation. The main symbols used in the formulation are summarized in Table 1.

2.1. Temperature and Humidity Control Scenario for Industrial Silkworm Rearing

The control problem considered here is temperature–humidity regulation and energy optimization over a single daily operating cycle of an industrial silkworm rearing workshop. A 15-min control interval is used, resulting in $T = 96$ decision steps per day. At each step, the controller selects equipment actions according to the current indoor state, external disturbances, electricity price, and process-induced thermal–humidity load. Energy use, comfort deviations, and switching behavior are then evaluated over the full day.

Unlike conventional building-control scenarios, the target environment in silkworm rearing depends on both the instar stage and production procedures. A stage variable $z_t \in \mathcal{Z}$ is therefore introduced. It links each control step to the corresponding comfort zone, safety zone, and process-load setting. Fig. 1 shows the typical workflow of the fifth-instar rearing stage. All formal experiments focus on this stage to ensure controlled comparisons, although the formulation can be extended to multi-stage control.

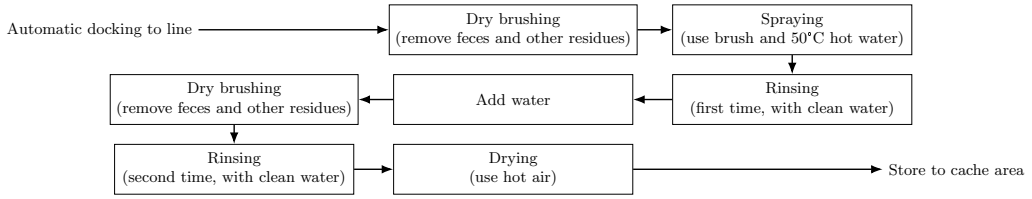

Fig. 1. Technical workflow of the fifth-instar rearing stage.

Table 1. Main symbols and physical interpretations.

Symbol	Physical Meaning
t	Basic control time step in the 96-step daily schedule
k	Current rolling instant
τ	Time-step index within the prediction horizon from k
T	Total daily control steps, with $T = 96$
T_p	MPC prediction horizon length, with $T_p = 6$ for EM local refinement
$\boldsymbol{x}_t$	Internal state vector with indoor states and previous control actions
$\boldsymbol{q}_t$	Process-induced thermal–humidity load vector
$\boldsymbol{w}_t$	External disturbance vector with weather, electricity prices, and process loads
z_t	Silkworm rearing and instar stage
$\boldsymbol{s}_t$	Controller-observable information composed of $\boldsymbol{x}_t$, $\boldsymbol{w}_t$, and z_t
$\boldsymbol{u}_t$	Real-time equipment control action
$\mathcal{A}$	Discrete feasible control action space formed by $\mathcal{A}^h$, $\mathcal{A}^v$, and $\mathcal{A}^d$
f_{EP}	EnergyPlus model that generates physically consistent simulation data
$\hat{f}_\theta$	Surrogate model for fast short-term prediction in rolling optimization
f_{eval}	Closed-loop evaluation environment for executed control performance
$\hat{\boldsymbol{y}}_{t+1}$	Predicted temperature and humidity response vector
$\mathcal{C}_z$	Comfort zone under specific rearing stage z
$\mathcal{S}_z$	Safety constraint zone under specific rearing stage z
E_t	Equivalent energy consumption per 15-min interval
C_t	Energy cost under the normalized electricity-price signal
$P^T_{\tau\|k}, P^H_{\tau\|k}$	Penalty terms for temperature and humidity deviation beyond comfort range
$P^{\Delta}_{\tau\|k}$	Penalty term for frequent equipment switching
$P^s_{\tau\|k}$	Safety-zone violation penalty term
$r_{\tau\|k}$	Composite priority score for critical-step selection
$\mathcal{K}_k$	Set of critical time steps selected within the current prediction horizon
$\mathcal{V}_{\tau\|k}$	Local feasible neighborhood at time step τ within the rolling horizon
δ_1, δ_2	Neighborhood radii for critical and non-critical time steps
η	Minimum acceptable performance improvement threshold

2.2. Definition of State Variables, Disturbances, Control Actions and Stage Variables

The internal system state at time instant t is defined as

$$\boldsymbol{x}_t = \left[T_t, H_t, u^h_{t-1}, u^v_{t-1}, u^d_{t-1}\right]^{\mathsf{T}}, \tag{1}$$

where T_t and H_t denote indoor air temperature and indoor relative humidity, respectively; u^h_{t-1}, u^v_{t-1}, and u^d_{t-1} represent the thermal regulation, ventilation, and dehumidification actions implemented at the previous time step. The state vector therefore includes both the current indoor environmental

state and the most recent actuator settings. Including the previous actions allows the controller to account for switching behavior and short-term thermal–humidity inertia.

The process-induced thermal–humidity load is formulated as

$$\boldsymbol{q}_t = \left[q_t^T, q_t^H\right]^{\mathsf{T}}, \tag{2}$$

in which q_t^T denotes process thermal load and q_t^H denotes process moisture load. These terms capture additional disturbances caused by silkworm metabolism, leaf moisture release, feeding and cleaning operations, staff activity, and auxiliary equipment. In the simulations, $\boldsymbol{q}_t$ followed enterprise-provided operating assumptions and scenario settings.

The external disturbance vector is defined as

$$\boldsymbol{w}_t = \left[T_t^o, H_t^o, c_t, q_t^T, q_t^H\right]^{\mathsf{T}}, \tag{3}$$

where T_t^o and H_t^o denote outdoor temperature and outdoor relative humidity, and c_t denotes the electricity price signal. The disturbance vector combines weather, price, and process loads because the controller must respond simultaneously to environmental forcing, economic pressure, and production-induced heat-moisture release. The observable information available to the controller at time t is expressed as

$$\boldsymbol{s}_t = \left[(\boldsymbol{x}_t)^{\mathsf{T}}, (\boldsymbol{w}_t)^{\mathsf{T}}, z_t\right]^{\mathsf{T}}. \tag{4}$$

This observable vector contains the information required for online decision-making: the current internal state, exogenous disturbances, and the current production stage.

The current control action is formulated as

$$\boldsymbol{u}_t = \left[u_t^h, u_t^v, u_t^d\right]^{\mathsf{T}}, \tag{5}$$

in which u_t^h, u_t^v, and u_t^d represent the gear levels of thermal regulation, ventilation, and dehumidification, respectively. Because the workshop equipment operates at discrete gear levels, the optimization problem is formulated over a discrete action space:

$$\mathcal{A}^h = \{0,1,2,3\}, \quad \mathcal{A}^v = \{0,1,2,3,4\}, \quad \mathcal{A}^d = \{0,1,2,3\}, \tag{6}$$

$$\mathcal{A} = \mathcal{A}^h \times \mathcal{A}^v \times \mathcal{A}^d, \qquad |\mathcal{A}| = 80. \tag{7}$$

In the adopted scenario, u_t^h represents four grades of thermal regulation intensity. Forced cooling is mainly achieved by increasing ventilation, so no separate negative cooling gear is defined. To reduce the initial search burden of the baseline solvers, a library of thirteen typical actions is first used to generate candidate sequences. The full action space $\mathcal{A}$, or its restricted neighborhoods, is then used for local refinement. All admissible actions are finally converted into scheduled inputs for the thermal regulation, ventilation, and dehumidification modules in EnergyPlus or the surrogate model.

2.3. EnergyPlus Simulation Model and Surrogate Prediction Model

The proposed framework combines an EnergyPlus co-simulation model with a surrogate prediction model. The simulation and prediction models are organized in three layers. First, the EnergyPlus model f_{EP} provides physically consistent simulation data and supports the construction of the evaluation environment. Second, the surrogate model $\hat{f}_\theta$ is trained from EnergyPlus-generated data and is used for fast short-term prediction inside the rolling optimizer. Third, f_{eval} denotes the closed-loop evaluation environment used to update the executed state and assess daily control performance. Accordingly, EnergyPlus provides the physical basis, the surrogate model provides online prediction efficiency, and f_{eval} provides a consistent closed-loop benchmark.

The surrogate model takes the current system state, control action, external disturbance, and stage variable as inputs and outputs the predicted temperature and humidity responses at the next time step:

$$\hat{\boldsymbol{y}}_{t+1} = \hat{f}_\theta(\boldsymbol{x}_t, \boldsymbol{u}_t, \boldsymbol{w}_t, z_t) = \left[\hat{T}_{t+1}, \hat{H}_{t+1}\right]^{\mathsf{T}}. \tag{8}$$

Training samples were collected from EnergyPlus-based scenario simulations, and the corresponding convergence curves are shown later. The surrogate model is trained from simulation data and used as a short-term predictor within the rolling optimization.

In implementation, $\hat{f}_\theta$ is used for fast look-ahead prediction within the rolling optimizer, whereas EnergyPlus supports scenario generation and physically consistent evaluation. This separation keeps online optimization efficient while retaining a physics-based closed-loop benchmark.

2.4. Rolling-Horizon MPC Optimization Formulation

A rolling-horizon MPC framework is used to implement the control procedure. At the current time instant k, the controller acquires the observable

state $\boldsymbol{s}_k$ and the predicted disturbance sequence over the horizon

$$\left\{\boldsymbol{w}_{\tau|k}\right\}_{\tau=k}^{k+T_p-1}. \tag{9}$$

The enhancement module (EM) uses a prediction horizon of $T_p = 6$, corresponding to 90 min. Here, t denotes the basic daily control step, k denotes the current rolling decision instant, and τ indexes the prediction window. Some internal candidate-generation procedures use shorter look-ahead depths, whereas the baseline sequence passed to EM is represented over the common T_p horizon for all comparative evaluations.

The finite-horizon optimization problem formulated at instant k is expressed as

$$\min_{\boldsymbol{u}_{k:k+T_p-1}} J_k = \sum_{\tau=k}^{k+T_p-1} \ell(\boldsymbol{x}_{\tau|k}, \boldsymbol{u}_{\tau|k}, \boldsymbol{w}_{\tau|k}, z_{\tau|k}). \tag{10}$$

where the instantaneous stage cost is defined by

$$\ell(\boldsymbol{x}_{\tau|k}, \boldsymbol{u}_{\tau|k}, \boldsymbol{w}_{\tau|k}, z_{\tau|k}) = C_{\tau|k} + \lambda_T P^T_{\tau|k} + \lambda_H P^H_{\tau|k} + \lambda_\Delta P^\Delta_{\tau|k} + P^s_{\tau|k}. \tag{11}$$

Equation (10) defines the rolling-horizon objective at instant k. The stage cost in Eq. (11) penalizes weighted energy cost, comfort-zone deviations, frequent switching, and any safety-zone violation within the prediction horizon.

The state update rules in rolling prediction are given as

$$\hat{\boldsymbol{y}}_{\tau+1|k} = \hat{f}_\theta(\boldsymbol{x}_{\tau|k}, \boldsymbol{u}_{\tau|k}, \boldsymbol{w}_{\tau|k}, z_{\tau|k}). \tag{12}$$

$$\boldsymbol{x}_{\tau+1|k} = g(\boldsymbol{x}_{\tau|k}, \boldsymbol{u}_{\tau|k}, \hat{\boldsymbol{y}}_{\tau+1|k}). \tag{13}$$

Only the first control action is implemented after optimization:

$$\boldsymbol{u}_k = \boldsymbol{u}^*_{k|k}. \tag{14}$$

The system state is then updated by the simulation environment, and the optimization problem in Eq. (10) is solved again at the next instant $k + 1$. All evaluations therefore focus on closed-loop control performance over the 96 rolling time steps rather than on offline global optimization with a fixed daily control strategy. This receding-horizon mechanism is important because weather conditions, electricity prices, and process loads may change the preferred action sequence from one control step to the next.

2.5. Definition of Comfort Zone, Safety Zone, Energy Cost and Penalty Terms

For any given rearing stage z, the comfort zone is defined as

$$\mathcal{C}_z = [\underline{T}_z, \overline{T}_z] \times [\underline{H}_z, \overline{H}_z]. \tag{15}$$

The safety zone is formulated as

$$\mathcal{S}_z = [\underline{T}^s_z, \overline{T}^s_z] \times [\underline{H}^s_z, \overline{H}^s_z], \qquad \mathcal{C}_z \subset \mathcal{S}_z. \tag{16}$$

For the fifth-instar scenario considered here, the comfort zone is set to 22.0–23.0 °C and 53.0%–58.0% relative humidity, while the safety zone is set to 20.0–26.0 °C and 45.0%–65.0%. These boundaries are determined based on enterprise-provided operating specifications and are kept identical for all algorithms. The two-layer design separates preferred operation from absolute safety: deviations from $\mathcal{C}_z$ are allowed but penalized, whereas leaving $\mathcal{S}_z$ is treated as unacceptable.

The equivalent energy consumption within each 15-min interval is defined as

$$E_t = \Delta t \left(P_h(u^h_t; T^o_t) + P_v(u^v_t) + P_d(u^d_t) + P_{base} \right), \qquad \Delta t = 0.25 \text{ h}. \tag{17}$$

Here, $P_h(\cdot)$, $P_v(\cdot)$, and $P_d(\cdot)$ denote the equivalent power consumption of the thermal regulation, ventilation, and dehumidification devices, respectively. The quantity E_t combines simulated thermal–humidity responses with actual gear settings and represents the equivalent per-step energy demand of the controlled equipment. Since the controller uses normalized electricity prices, the weighted energy cost is written as

$$C_t = c_t E_t. \tag{18}$$

Here, C_t denotes the weighted energy cost under the normalized price signal. It is therefore distinct from the RMB-based economic estimates reported later in the engineering assessment.

The temperature and humidity comfort penalties are formulated as

$$P^T_{\tau|k} = \left[\max\left(0, \hat{T}_{\tau|k} - \overline{T}_{z_{\tau|k}}\right) + \max\left(0, \underline{T}_{z_{\tau|k}} - \hat{T}_{\tau|k}\right) \right]^2. \tag{19}$$

The quadratic form assigns larger penalties to larger temperature deviations beyond the comfort zone.

$$P^H_{\tau|k} = \left[\max\left(0, \hat{H}_{\tau|k} - \overline{H}_{z_{\tau|k}}\right) + \max\left(0, \underline{H}_{z_{\tau|k}} - \hat{H}_{\tau|k}\right) \right]^2. \tag{20}$$

The humidity penalty is defined analogously.

The equipment switching penalty is given by

$$P^{\Delta}_{\tau|k} = \left\| \boldsymbol{u}_{\tau|k} - \boldsymbol{u}_{\tau-1|k} \right\|_1 . \tag{21}$$

This term penalizes frequent gear changes and promotes a smoother actuator schedule. Here, the L_1 distance over discrete gear levels is used as a proxy for switching intensity rather than a measured startup-loss model.

When the predicted temperature or humidity falls outside the predefined safety zone, a large penalty term is imposed as

$$P^{s}_{\tau|k} = M \cdot \mathbb{I}\left[\left(\hat{T}_{\tau|k}, \hat{H}_{\tau|k} \right) \notin \mathcal{S}_{z_{\tau|k}} \right] . \tag{22}$$

Here, M is a sufficiently large constant. Unsafe candidates are therefore strongly disfavored during the search.

To evaluate daily comfort satisfaction, the comfort satisfaction rate (CR) is defined as

$$\mathrm{CR} = \frac{1}{T} \sum_{t=1}^{T} \mathbb{I}\left[(T_t, H_t) \in \mathcal{C}_{z_t} \right] . \tag{23}$$

The safety violation rate (SVR) is expressed as

$$\mathrm{SVR} = \frac{1}{T} \sum_{t=1}^{T} \mathbb{I}\left[(T_t, H_t) \notin \mathcal{S}_{z_t} \right] . \tag{24}$$

The unified penalty weights are set as $\lambda_T = 0.5$, $\lambda_H = 0.024$ and $\lambda_\Delta = 0.08$. They were calibrated on six tuning scenarios and then kept fixed for all algorithms and all eighteen formal evaluation cases. These weights balance the scales of temperature deviation, humidity deviation, switching, and energy cost without case-specific retuning.

2.6. Deterministic Priority Indicator and Critical Time Step Identification

The priority-guided mechanism in this work is not a chance-constrained or stochastic MPC formulation in a strict probabilistic sense. It defines a deterministic priority rule based on boundary margins, electricity price levels, process loads, and action variation to identify the time steps that warrant additional local search effort.

At control instant k, the integrated priority score for each time step $\tau \in \{k, \ldots, k + T_p - 1\}$ within the prediction horizon is calculated by

$$r_{\tau|k} = \alpha_T r^{T}_{\tau|k} + \alpha_H r^{H}_{\tau|k} + \alpha_c r^{c}_{\tau|k} + \alpha_q r^{q}_{\tau|k} + \alpha_\Delta r^{\Delta}_{\tau|k}. \tag{25}$$

where $\alpha_T, \alpha_H, \alpha_c, \alpha_q, \alpha_\Delta \geq 0$ and

$$\alpha_T + \alpha_H + \alpha_c + \alpha_q + \alpha_\Delta = 1. \tag{26}$$

Each component reflects a different source of control difficulty: proximity to safety boundaries, high-price electricity periods, strong process loads, and abrupt action changes.

The temperature and humidity boundary risk indexes are written as

$$r^T_{\tau|k} = 1 - \frac{\min\left(\hat{T}_{\tau|k} - \underline{T}^s_{z_{\tau|k}}, \overline{T}^s_{z_{\tau|k}} - \hat{T}_{\tau|k}\right)}{\overline{T}^s_{z_{\tau|k}} - \underline{T}^s_{z_{\tau|k}} + \epsilon}. \tag{27}$$

$$r^H_{\tau|k} = 1 - \frac{\min\left(\hat{H}_{\tau|k} - \underline{H}^s_{z_{\tau|k}}, \overline{H}^s_{z_{\tau|k}} - \hat{H}_{\tau|k}\right)}{\overline{H}^s_{z_{\tau|k}} - \underline{H}^s_{z_{\tau|k}} + \epsilon}. \tag{28}$$

in which $\epsilon > 0$ denotes a tiny constant to avoid division by zero. The electricity price risk is defined as

$$r^c_{\tau|k} = \frac{c_{\tau|k} - c_{\min}}{c_{\max} - c_{\min} + \epsilon}. \tag{29}$$

The process load risk is formulated as

$$r^q_{\tau|k} = \frac{\left\|\boldsymbol{q}_{\tau|k}\right\|_2 - q_{\min}}{q_{\max} - q_{\min} + \epsilon}. \tag{30}$$

Here, $q_{\min}$ and $q_{\max}$ denote the minimum and maximum values of $\|\boldsymbol{q}_{\tau|k}\|_2$ in the normalized scenario set.

The action fluctuation risk is expressed as

$$r^\Delta_{\tau|k} = \frac{\left\|\boldsymbol{u}^b_{\tau|k} - \boldsymbol{u}^b_{\tau-1|k}\right\|_1}{\Delta_{\max} + \epsilon}, \tag{31}$$

where $\boldsymbol{u}^b_{\tau|k}$ denotes the baseline control action at time step τ. A larger integrated score indicates that the corresponding step is closer to a safety boundary, coincides with a higher electricity price, experiences a stronger process load, or involves a larger action change.

After obtaining the priority scores, the set of critical time steps within the current rolling horizon is defined as

$$\mathcal{K}_k = \left\{\tau \in \{k, \ldots, k + T_p - 1\} : r_{\tau|k} \text{ ranks among the top } K\right\}. \tag{32}$$

and the set of non-critical time steps is expressed as

$$\bar{\mathcal{K}}_k = \{k, \ldots, k + T_p - 1\} \setminus \mathcal{K}_k. \tag{33}$$

Selecting only the top-K priority-ranked steps concentrates the computational budget on the parts of the horizon where local refinement is most likely to be effective. The remaining steps still follow the baseline schedule or a restricted neighborhood, depending on the search mode.

3. Proposed Method

Based on the formulation above, this section introduces the priority-guided local refinement strategy used to improve baseline heuristic control sequences. Here, local refinement denotes the overall EM adjustment stage, while restricted neighborhoods and hotspot expansion denote two mechanisms used within that stage. For concise presentation, the integrated procedure is referred to as the priority-guided search strategy.

3.1. Baseline Heuristic Control Sequence Generation

Five baseline solvers are used for comparative experiments: a rule-based strategy (RB), tabu search (TS), simulated annealing (SA), a genetic algorithm (GA), and particle swarm optimization (PSO). At each control instant k, all baseline methods use the same observed state $\boldsymbol{s}_k$, predicted horizon information $\{\boldsymbol{w}_{\tau|k}, z_{\tau|k}\}$, feasible action space $\mathcal{A}$, and objective function in Eq. (10). Each method then generates a baseline control sequence

$$\boldsymbol{u}^b_{k:k+T_p-1} = \left[\boldsymbol{u}^b_{k|k}, \ldots, \boldsymbol{u}^b_{k+T_p-1|k}\right]. \tag{34}$$

The EM refinement layer does not act as an independent optimizer; instead, it performs local refinement on preliminary baseline solutions.

3.2. Priority-Guided Critical Time Step Selection

Once the baseline sequences are available, the surrogate model generates rolling predictions $\hat{\boldsymbol{y}}_{\tau|k}$, and the priority score for each step is computed using Eq. (25). All steps are then sorted in descending order, and the top K are selected to form the critical set $\mathcal{K}_k$. The resulting procedure allocates the available computational budget to the time steps with the greatest boundary pressure, energy-cost pressure, or disturbance intensity.

3.3. Restricted Neighborhood Construction: RIGID and FLEX Modes

For each critical time step $\tau \in \mathcal{K}_k$, a local neighborhood centered on the baseline action $\boldsymbol{u}^b_{\tau|k}$ is established as

$$\mathcal{V}_{\tau|k} = \left\{ \tilde{\boldsymbol{u}}_{\tau|k} \in \mathcal{A} : d(\tilde{\boldsymbol{u}}_{\tau|k}, \boldsymbol{u}^b_{\tau|k}) \leq \delta_1 \right\}. \tag{35}$$

where $d(\cdot, \cdot)$ denotes the L_∞ distance defined over discrete gear indices. Because all control variables are discrete gear levels, additional dimensional normalization is unnecessary. The critical-step neighborhood therefore permits targeted local adjustment without searching the entire combinatorial action space.

Two restricted-neighborhood modes, namely RIGID and FLEX, are applied to non-critical time steps $\tau \in \bar{\mathcal{K}}_k$. Under the RIGID strategy,

$$\bar{\mathcal{V}}_{\tau|k} = \left\{ \boldsymbol{u}^b_{\tau|k} \right\}. \tag{36}$$

Under RIGID, non-critical steps remain fixed at their baseline values, whereas FLEX allows small adjustments with a smaller radius than that used for critical steps. Under the FLEX strategy,

$$\bar{\mathcal{V}}_{\tau|k} = \left\{ \tilde{\boldsymbol{u}}_{\tau|k} \in \mathcal{A} : d(\tilde{\boldsymbol{u}}_{\tau|k}, \boldsymbol{u}^b_{\tau|k}) \leq \delta_2 \right\}, \qquad \delta_2 < \delta_1. \tag{37}$$

This design expands the search only where refinement is most useful while preserving the overall structure of the baseline solution.

3.4. Candidate Ranking, Heuristic Pruning Estimate, and Hotspot Expansion Rule

Candidate ranking is performed before combinatorial search so that not all actions in the critical neighborhoods need to be retained. For any candidate action $\tilde{\boldsymbol{u}}_{\tau|k}$, the local evaluation score is defined as

$$\Gamma(\tilde{\boldsymbol{u}}_{\tau|k}) = \beta_J \Delta\ell_{\tau|k} + \beta_r r_{\tau|k} + \beta_\Delta \left\| \tilde{\boldsymbol{u}}_{\tau|k} - \boldsymbol{u}^b_{\tau|k} \right\|_1. \tag{38}$$

in which

$$\Delta\ell_{\tau|k} = \ell(\boldsymbol{x}_{\tau|k}, \tilde{\boldsymbol{u}}_{\tau|k}, \boldsymbol{w}_{\tau|k}, z_{\tau|k}) - \ell(\boldsymbol{x}_{\tau|k}, \boldsymbol{u}^b_{\tau|k}, \boldsymbol{w}_{\tau|k}, z_{\tau|k}). \tag{39}$$

Here, $r_{\tau|k}$ sets the priority of the time step, whereas candidate-level differentiation within the same step is mainly driven by the local cost change and

the deviation from the baseline action. Only the top N_c candidates with the best scores are retained for the subsequent combinatorial search. The ranking stage reduces branching before the more expensive local sequence search begins. The nonnegative weights β_J, β_r, and β_Δ balance local cost change, time-step priority, and deviation from the baseline action, respectively.

A heuristic pruning estimate is introduced during the branch search procedure. Once the first m local actions are fixed, the optimistic estimated cost for the remaining undetermined set $\mathcal{R}_m$ is derived as

$$LB_m = J_{\text{fixed},m} + \sum_{\tau \in \mathcal{R}_m} \min_{\tilde{\boldsymbol{u}} \in \mathcal{V}_{\tau|k}} \ell(\boldsymbol{x}_{\tau|k}, \tilde{\boldsymbol{u}}, \boldsymbol{w}_{\tau|k}, z_{\tau|k}). \tag{40}$$

where $J_{\text{fixed},m}$ represents the accumulated cost of the confirmed local actions. If $LB_m \geq J_{\text{best}}$, the branch is truncated in advance. This screening estimate is heuristic and is used to remove clearly inferior branches at an early stage.

If the performance improvement obtained from the initial local refinement is smaller than the preset threshold η, namely

$$J_k(\boldsymbol{u}^b_{k:k+T_p-1}) - J_k(\tilde{\boldsymbol{u}}_{k:k+T_p-1}) \leq \eta. \tag{41}$$

an adjacent-step expansion rule, hereafter referred to as hotspot expansion, is applied around the highest-priority time step τ^*:

$$\mathcal{K}'_k = \mathcal{K}_k \cup \{\tau^* - 1, \tau^* + 1\}. \tag{42}$$

Boundary-index correction is then performed, followed by another round of local search. This expansion accounts for the temporal coupling of temperature–humidity responses across adjacent steps.

3.5. Complete Rolling Control Framework

With the critical time-step set and local feasible neighborhoods defined, the restricted local-search problem is formulated as

$$\begin{aligned} \min_{\tilde{\boldsymbol{u}}_{k:k+T_p-1}} \quad & J_k(\tilde{\boldsymbol{u}}_{k:k+T_p-1}) \\ \text{s.t.} \quad & \tilde{\boldsymbol{u}}_{\tau|k} \in \mathcal{V}_{\tau|k}, \quad \tau \in \mathcal{K}_k, \\ & \tilde{\boldsymbol{u}}_{\tau|k} \in \bar{\mathcal{V}}_{\tau|k}, \quad \tau \in \bar{\mathcal{K}}_k. \end{aligned} \tag{43}$$

Within this framework, the preceding equations define the rolling-horizon objective, critical time-step identification, restricted neighborhoods, candidate screening, and the final restricted local-search problem. Algorithm 1 integrates these components into a single closed-loop control procedure.

Algorithm 1 Rolling control procedure of the priority-guided local refinement strategy.

Input: $\boldsymbol{x}_k$, $\boldsymbol{s}_k$, $\{\boldsymbol{w}_{\tau|k}\}_{\tau=k}^{k+T_p-1}$, $\{z_{\tau|k}\}_{\tau=k}^{k+T_p-1}$, baseline heuristic, and $K, \delta_1, \delta_2, N_c, \eta$.
Output: Real-time control action $\boldsymbol{u}_k$.
Generate a baseline control sequence $\boldsymbol{u}^b_{k:k+T_p-1}$ using the selected baseline heuristic algorithm.
for $\tau = k$ to $k + T_p - 1$ **do**
    Obtain the predicted state $\hat{\boldsymbol{y}}_{\tau+1|k} = \hat{f}_\theta(\boldsymbol{x}_{\tau|k}, \boldsymbol{u}^b_{\tau|k}, \boldsymbol{w}_{\tau|k}, z_{\tau|k})$ using the surrogate model.
    Calculate the corresponding priority score $r_{\tau|k}$.
end for
Select the top K high-priority time steps to construct the critical set $\mathcal{K}_k$.
Establish local neighborhoods $\mathcal{V}_{\tau|k}$ for critical steps and RIGID/FLEX restricted neighborhoods $\bar{\mathcal{V}}_{\tau|k}$ for non-critical steps.
Implement candidate ranking for feasible actions at critical steps and retain the top N_c qualified candidates.
Conduct local combinatorial search with the heuristic pruning estimate to obtain the refined sequence $\tilde{\boldsymbol{u}}_{k:k+T_p-1}$.
if $J_k(\boldsymbol{u}^b_{k:k+T_p-1}) - J_k(\tilde{\boldsymbol{u}}_{k:k+T_p-1}) \leq \eta$ **then**
    Perform hotspot expansion around the highest-priority time step and repeat the local search.
end if
if $J_k(\boldsymbol{u}^b_{k:k+T_p-1}) - J_k(\tilde{\boldsymbol{u}}_{k:k+T_p-1}) > \eta$ **then**
    Adopt the optimized control sequence.
else
    Retain the original baseline sequence.
end if
Execute only the first control action $\boldsymbol{u}_k = \tilde{\boldsymbol{u}}_{k|k}$ or $\boldsymbol{u}^b_{k|k}$.
Update the workshop environmental states via f_{eval} and proceed to the next rolling instant $k + 1$.

4. CPES Integration and Data Interface

This section embeds the formulation and refinement strategy into the CPES data flow. It clarifies how state acquisition, disturbance access, model invocation, optimizer output, and feedback update are connected in the closed-loop CPES implementation.

4.1. State Acquisition

In the closed-loop implementation, the primary role of the CPES is to provide the observable state $\boldsymbol{s}_t$ to the controller. The workshop collects real-time temperature, humidity, and recent equipment-operation records. Gateways and databases aggregate and cache these data, after which the controller reconstructs $\boldsymbol{x}_t$ and the previous actions. Fig. 2 illustrates the corresponding acquisition structure. This interface definition supports closed-loop simulation and standardized data exchange.

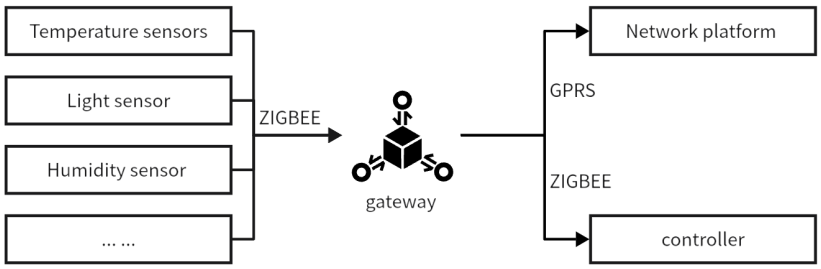

Fig. 2. Integrated intelligent monitoring and environmental control system for silkworm rearing.

4.2. Access of Meteorological Data, Electricity Price and Process Thermal-Humidity Load

This subsection describes the data categories required by the CPES interface. The disturbance vector $\boldsymbol{w}_t$ consists of three components: public meteorological data resampled from hourly resolution to 15-min intervals, public electricity price data processed into normalized price sequences, and process-induced thermal–humidity loads derived from enterprise-provided operating parameters. The load scenarios follow the production rules of fifth-instar rearing. The resulting platform is a scenario-driven evaluation system that combines enterprise-provided parameters, public disturbance data, and co-simulation-based prediction. The detailed sampling, filtering, and scenario partitioning procedure used in the numerical experiments is reported later in Section 5.1.

4.3. Invocation of EnergyPlus and Surrogate Prediction Model

Within the closed-loop data flow, the controller first uses the trained surrogate model $\hat{f}_\theta$, together with the observed state $\boldsymbol{s}_k$ and predicted disturbances, to obtain short-term temperature and humidity trajectories over the prediction horizon. The local refinement modules then revise the baseline sequence, and the closed-loop state update is completed by f_{eval}. Fig. 3 summarizes this interaction. In this framework, the surrogate model supports fast online prediction, while EnergyPlus provides the physical basis for the evaluation environment.

4.4. Optimizer Output and System State Feedback

The optimizer outputs the instantaneous action $\boldsymbol{u}_k$ at time k. This action is transmitted to the execution layer and incorporated into $\boldsymbol{x}_{k+1}$ for the next

iteration. Each executed action affects subsequent energy cost, switching penalty, and environmental constraint pressure. The CPES framework thus provides a closed-loop interaction structure that links sensing, disturbance input, prediction, and optimization.

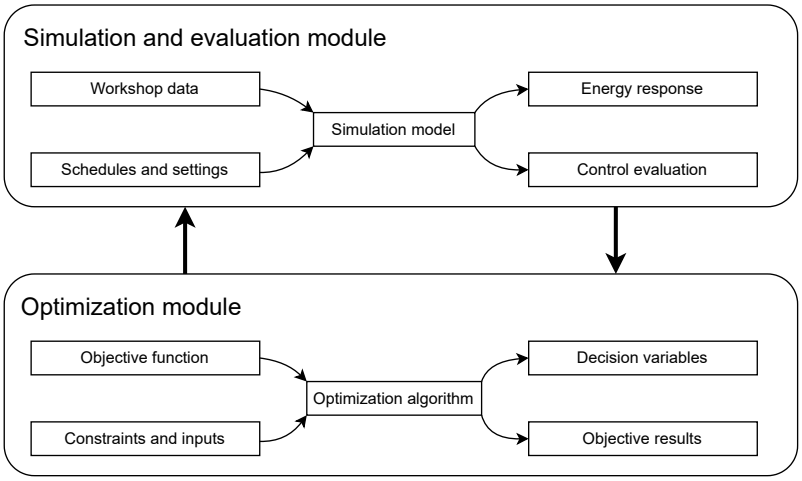

Fig. 3. Cooperative solution flow between the EM strategy and the co-simulation platform.

5. Numerical Validation and Industry-Parameter-Based Case Study

This section evaluates the proposed framework in two parts: closed-loop numerical validation and a separate enterprise-parameter-based engineering assessment. The main effectiveness analysis is based on paired comparisons across eighteen formal evaluation scenarios. The engineering assessment provides scheme-level estimates under specified parameters and assumptions.

5.1. Data Source and Scenario Establishment

Building on the data-interface definition in Section 4.2, this subsection specifies how the numerical dataset was constructed for calibration and formal evaluation. All experiments use a scenario-driven dataset constructed from enterprise-provided parameters, public disturbance data, and co-simulation responses. The public meteorological and electricity price data cover the year

2024 at hourly resolution, with 8784 original records. After synchronization to the 15-min control interval and data-validity filtering, 263 valid daily samples remained. To separate calibration from testing, 24 daily scenarios were sampled: 6 were used for penalty-weight adjustment and hyperparameter tuning, and the remaining 18 were reserved for formal evaluation without secondary retuning.

EnergyPlus co-simulation runs at 15-min intervals, so each daily scenario contains 96 state transitions. All formal experiments focus on fifth-instar rearing with fixed stage settings, although the formulation remains extendable to other stages. The experiments use the common receding-horizon setting with $T_p = 6$, corresponding to a 90-min prediction window.

A relatively narrow comfort zone is used to make performance differences among controllers observable. These comfort limits are used only for soft penalties and comfort-satisfaction statistics, while the fixed safety limits of 20.0–26.0 °C and 45.0%–65.0% remain unchanged across all experiments. The full evaluation set contains 18 daily scenarios and 10 algorithm variants, corresponding to $18 \times 96 \times 10 = 17280$ state-transition assessments.

5.2. Experimental Protocol and Parameter Configuration

For a fair comparison, all baseline heuristics and their EM-enhanced variants use the same state inputs, feasible action spaces, surrogate prediction framework, optimization objective, and safety constraints in every formal evaluation scenario. Hyperparameters were tuned automatically on the six calibration scenarios. The penalty weights λ_T, λ_H, and λ_Δ were also fixed after calibration and were not adjusted again in the formal tests.

Because the EM refinement layer adds local refinement after baseline sequence generation, it uses more computation than the original solvers. Accordingly, the comparison evaluates both performance improvement and online compatibility within the 15-min control interval. In the hyperparameter calibration procedure, each candidate parameter setting is evaluated through the corresponding optimization run, its composite objective value is recorded as the fitness indicator, and the search is updated iteratively until the stopping condition is satisfied.

In this framework, the average composite objective on the calibration scenarios was used as the unified criterion for selecting parameter combinations. The search procedure identified high-performing configurations with fewer trials than an exhaustive grid search.

Fig. 4 and Fig. 5 show the convergence of the surrogate models on the EnergyPlus-generated training data. These curves indicate stable training behavior and provide a preliminary basis for using the surrogate models in short-term rolling prediction. Their generalization to long-term field operation still requires independent validation with measured data.

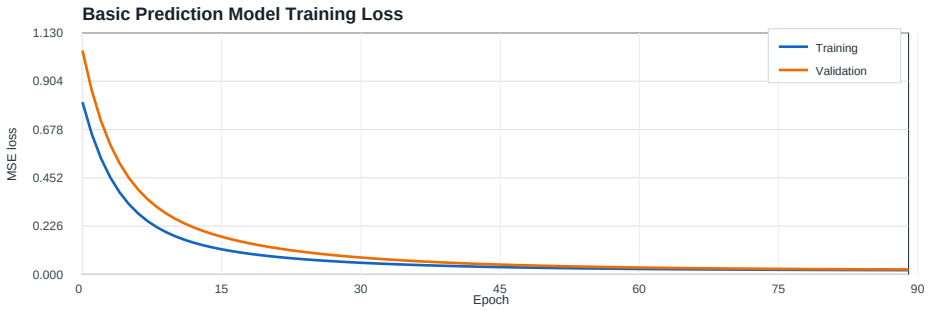

Fig. 4. Training convergence of the basic surrogate model on the simulation dataset.

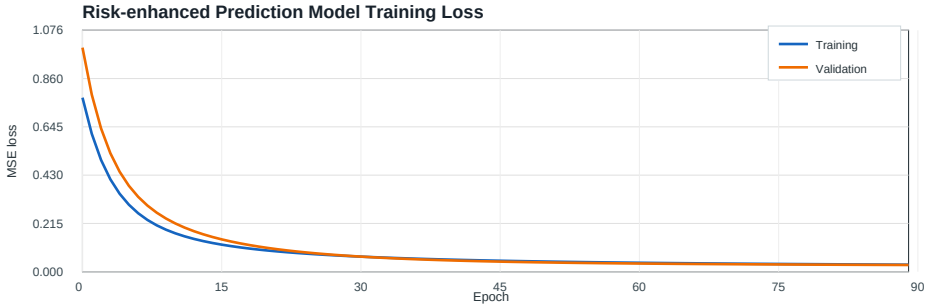

Fig. 5. Training convergence of the priority-enhanced surrogate model on the simulation dataset.

5.3. Comparative Analysis of Control Performance among Multiple Algorithms

Five baseline algorithms and their five EM-enhanced counterparts were compared across the eighteen formal evaluation scenarios. The evaluation metrics were the composite objective, energy cost, comfort satisfaction rate, temperature penalty, humidity penalty, and switching penalty. Fig. 6 and

Fig. 7 show representative temperature and humidity trajectories. The baseline methods deviate from the comfort zone during some periods, whereas the EM-enhanced strategies adjust the control sequence more effectively near the comfort boundaries.

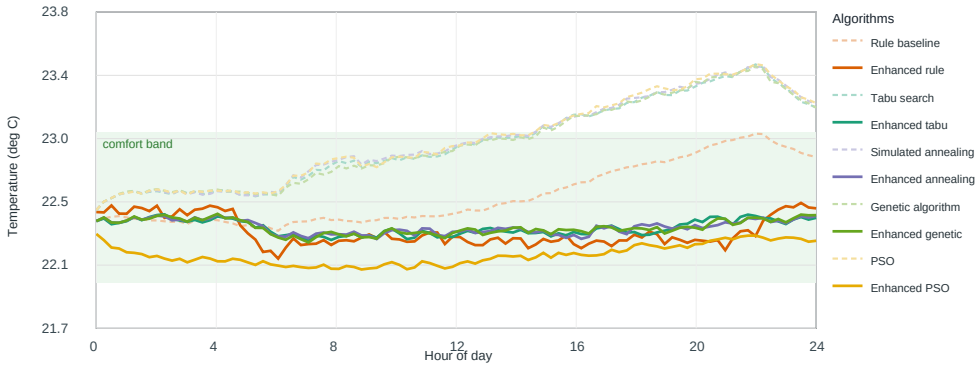

Fig. 6. Representative temperature-control trajectories under selected evaluation scenarios (solid lines: EM-enhanced strategies; dashed lines: baseline methods; shaded areas: comfort zones).

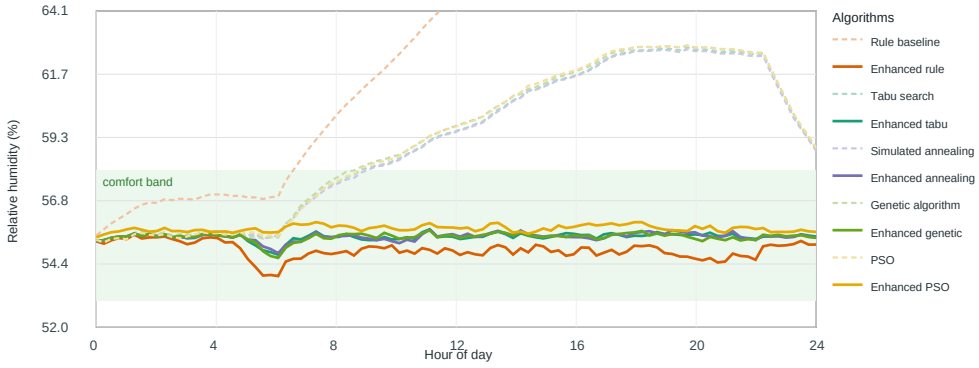

Fig. 7. Representative humidity-control trajectories under selected evaluation scenarios (solid lines: EM-enhanced strategies; dashed lines: baseline methods; shaded areas: comfort zones).

Table 2 summarizes the average results of all ten algorithms across the eighteen scenarios. All EM-enhanced variants achieved lower average composite objective values than their corresponding baselines, with improvement

ratios ranging from 31.04% to 59.56%. Among the ten main baseline and EM-enhanced methods, EM-PSO attained the lowest average composite objective value, 514.94.

The main source of this improvement was the reduction in comfort-boundary penalties. All EM-enhanced strategies reached a comfort satisfaction rate of 1.0000, and their temperature and humidity penalties were reduced to zero. The results suggest that the proposed priority-based critical-step identification and local refinement primarily improve constraint satisfaction near the comfort-zone boundaries.

The improvement also involves trade-offs. Energy cost did not decrease in every EM variant, and switching penalties increased in several cases. For example, EM-RB reduced the composite objective value from 1354.92 to 547.94, but raised energy cost from 416.76 to 539.13 and switching penalty from 30.00 to 110.11. Overall, EM refinement improves the composite objective and comfort-control stability without consistently improving every individual metric.

All EM-enhanced strategies outperformed their corresponding baseline methods in terms of average composite objective values within the established test cases. Table 3 further summarizes the average optimization improvement magnitude and changes in comfort satisfaction rate for the five paired comparison groups.

Table 2. Average control performance of the compared algorithms over eighteen formal evaluation scenarios.

Algorithm	Composite objective	Energy cost	Comfort satisfaction rate	Temperature penalty	Humidity penalty	Switching penalty
RB	1354.92	416.76	0.2772	96.78	36973.82	30.00
EM-RB	547.94	539.13	1.0000	0.00	0.00	110.11
TS	823.76	516.18	0.4850	143.17	9660.07	51.92
EM-TS	536.46	527.85	1.0000	0.00	0.00	107.69
SA	820.75	517.02	0.4826	147.97	9397.30	52.67
EM-SA	553.15	543.44	1.0000	0.00	0.00	121.47
GA	817.96	516.27	0.4682	142.41	9430.79	51.83
EM-GA	564.04	554.51	1.0000	0.00	0.00	119.19
PSO	835.09	515.30	0.4774	149.65	10031.73	52.47
EM-PSO	514.94	507.53	1.0000	0.00	0.00	92.58

Table 3. Improvements in composite objective values achieved by EM-enhanced strategies over baseline algorithms across eighteen scenarios.

Comparison group	Baseline objective	EM objective	Objective improvement (%)	Comfort satisfaction rate change
RB → EM-RB	1354.92	547.94	59.56%	0.2772 → 1.0000
TS → EM-TS	823.76	536.46	34.88%	0.4850 → 1.0000
SA → EM-SA	820.75	553.15	32.60%	0.4826 → 1.0000
GA → EM-GA	817.96	564.04	31.04%	0.4682 → 1.0000
PSO → EM-PSO	835.09	514.94	38.34%	0.4774 → 1.0000

5.4. Mechanism Verification and Ablation Study Results

To clarify the roles of the priority-identification module and the restricted-neighborhood settings, ablation experiments were conducted using PSO as the representative baseline. Table 4 reports the results. These tests isolate the contributions of the priority-identification module and the restricted-neighborhood settings.

The original PSO algorithm yielded a composite objective value of 835.09 and a large combined temperature–humidity penalty of 10181.38. After adding only the priority-identification mechanism, PSO+Risk reduced the composite objective value to 510.05 and reached a comfort satisfaction rate of 1.0000. This result shows that priority-based critical-step identification was the main driver of the observed improvement. PSO+RNS-Rigid, PSO+RNS-Flex, and PSO+RNS-Branch obtained composite objective values of 514.88, 512.21, and 517.28, respectively, all with full comfort satisfaction. The neighborhood variants mainly adjusted the trade-off between energy cost and switching cost.

Both PSO+Risk and PSO+RNS-Flex achieved lower composite objective values than EM-PSO, whose value was 514.94. Within this ablation set, the complete EM-PSO configuration therefore does not show additive improvement over the strongest single-module variants. The main result of the paper remains the paired improvement of each EM-enhanced solver over its corresponding baseline in the ten-method comparison.

5.5. Significance Test and Computational Efficiency Analysis

The ablation study above compares internal PSO-derived variants and is used to identify the source of the improvement. The following significance

Table 4. Ablation results of PSO-based local refinement strategies across eighteen scenarios.

Method	Composite objective	Energy cost	Comfort satisfaction rate	Temperature–humidity penalty	Switching penalty
PSO	835.09	515.30	0.4774	10181.38	52.47
PSO+Risk	510.05	502.76	1.0000	0.00	91.14
PSO+RNS-Rigid	514.88	507.47	1.0000	0.00	92.67
PSO+RNS-Flex	512.21	504.87	1.0000	0.00	91.78
PSO+RNS-Branch	517.28	509.89	1.0000	0.00	92.31
EM-PSO	514.94	507.53	1.0000	0.00	92.58

tests return to the main experimental comparison, where EM-PSO is compared with the predefined baseline algorithms TS, SA, GA, and PSO across the eighteen formal scenarios.

Runtime statistics are reported in Table 5. All EM-enhanced strategies required more computation than their original baselines because they performed additional local refinement. For PSO, the average runtime per scenario increased from 2.85 s to 10.49 s, equivalent to about 0.1092 s per control step. Across all EM methods, the average single-step runtime remained between 0.0641 s and 0.1092 s, which is far shorter than the 15-min control interval. The added computation is therefore acceptable in the present surrogate-based closed-loop setting. Practical field delays, however, will still depend on communication, database access, actuator response, and control-platform implementation.

Table 5. Average computational runtime across eighteen formal evaluation scenarios.

Algorithm	Average time per scenario (s)	Average time per step (s)
RB	0.20	0.0021
TS	1.01	0.0105
SA	1.04	0.0108
GA	1.94	0.0202
PSO	2.85	0.0297
EM-RB	6.16	0.0641
EM-TS	8.59	0.0895
EM-SA	8.71	0.0908
EM-GA	9.59	0.0999
EM-PSO	10.49	0.1092

To test whether the advantage of EM-PSO was consistent across scenarios rather than caused by random fluctuations, Wilcoxon signed-rank tests were conducted on scenario-level composite objective values between EM-PSO and TS, SA, GA, and standard PSO. Table 6 reports the scenario means and two-tailed p-values.

The Wilcoxon results show that EM-PSO achieved significantly lower composite objective values than PSO, GA, SA, and TS within the eighteen-scenario evaluation set.

Together with the ablation results, these findings support the effectiveness of the proposed priority-guided local refinement strategy within the current eighteen-scenario simulation setting. Priority-based critical-step identification is the main source of improvement, whereas the complete EM configuration is not uniformly superior within the PSO-derived ablation set. Broader scenario sets and field data are still needed before extending the conclusions to wider annual operating conditions.

5.6. Engineering Assessment Based on Enterprise-Provided Parameters

The preceding subsections validate the proposed rolling control strategy under 15-min closed-loop scenarios. In contrast, this subsection provides a separate engineering pre-evaluation based on enterprise-provided aggregated parameters. This assessment is separated from the 15-min closed-loop MPC validation and evaluates scheme-level energy performance under specified workshop, equipment, and operation assumptions.

The engineering case is defined by the workshop layout, production process, and equipment parameters. Building characteristics affect the indoor thermal response and, in turn, the control outcome. Before defining the two operation schemes, the engineering inputs used to construct the workshop model are summarized in Tables 7–11. These tables provide the parameter

Table 6. Wilcoxon signed-rank tests between EM-PSO and baseline algorithms across eighteen formal evaluation scenarios.

Comparison pair	Baseline scenario mean	EM-PSO scenario mean	Improvement ratio (%)	Two-tailed p-value
PSO vs. EM-PSO	835.09	514.94	38.34	0.0040
GA vs. EM-PSO	817.96	514.94	37.05	0.0040
SA vs. EM-PSO	820.75	514.94	37.26	0.0047
TS vs. EM-PSO	823.76	514.94	37.49	0.0047

basis for the subsequent scheme comparison. Table 7 lists the basic building parameters, while Tables 8 and 9 summarize the heating, ventilation, and air-conditioning (HVAC), electrical, and mechanical equipment. Here, AHU denotes air handling unit, FL denotes fluorescent lamp, and CMH denotes cubic meters per hour. The parameters were provided by the cooperating enterprise, with some values supported by on-site measurement. For confidentiality, only aggregated information is reported in the main text.

Table 7. Structural components of the workshop building.

Building structure	**Quantity**	**Specification**
Wall	4	100 mm
Roof	1	25 mm
Floor	1	200 mm
Window	None	–
Pipeline	6	20, 40, 60 mm

Table 8. Specifications of the HVAC system and electrical equipment.

Category	**Equipment Item**	**Quantity**	**Capacity**	**Power**
HVAC system	Heating equipment	1	AHU 80000 CMH	22 kW
	Cooling equipment	1	AHU 80000 CMH	22 kW
	Ventilation equipment	6	AHU 10200 CMH	1.5 kW/unit
Electrical equipment	Production-line lighting	150	FL 2/32W	–
	Office-area lighting	20	FL 4/32W	–
	Other equipment	2	–	20 W

Table 9. Summary of mechanical equipment.

Equipment Item		Power (kW)	Quantity
Mechanical equipment	Water pump	60	2
	Sludge system pump	80	2
	Burner blower	3	2
	AirSeal	15	2
	Robot	100	8
	Conveyor	60	2
	Lifter #1	7.5	2
	Lifter #2	5.5	2
	Heater1	120	2
	Heater2	120	3
	Refrigeration unit	100	2

Based on Tables 7–9, the corresponding simulation components are determined and summarized in Tables 10 and 11. The relevant data are then integrated into the enterprise workshop model.

These tables establish the mapping from engineering parameters to simulation objects. Tables 10 and 11 translate the building and equipment descriptions into components that can be directly recognized by the energy model.

Within this engineering assessment, two termination criteria are used in the optimization process. The algorithm stops if no further improvement is found within 100 consecutive iterations or after 24,000 iterations in total.

Table 10. Simulation components of the workshop building, equipment, HVAC system, and production schedule.

Purpose	Type	Description	Simulation Component	Quantity
Building structure	Wall	Reinforced concrete	ZONE SURFACE WEST, etc.	4
	Floor	Reinforced concrete	ZONE SURFACE FLOOR	1
	Roof	Reinforced concrete	ZONE SURFACE ROOF	1
Pipeline	Gas pipe	Gas pipeline	Heating Supply Side Bypass, etc.	6
	Air duct	Air pipeline	Supply Air Temp Nodes, etc.	3
	Water pipe	Water pipeline	Water Heater Use Outlet Pipe, etc.	2
Equipment	Electrical equipment	Lighting	ZONE ONE Lights1, etc.	150
	Other equipment	Broadcasting system	–	1
HVAC system	Mechanical equipment	Gas heating equipment	Gas Heater1, Gas Heater2	2
	Gas system	Gas heating system	Coil:Heating:Gas	1
	Power system	Other equipment	Conveyor, Lifter, Robot, etc.	60
	Heating	Heating system	Coil:Heating:Gas	1
	Cooling	Cooling system	Coil:Cooling:DX:SingleSpeed	1
	Ventilation system	Ventilation equipment	Exhaust Fan1, 2, 3, 4, 5, 6, 7	7
Other	Production schedule	Painting schedule, etc.	–	8

Production schedules are modeled as discrete variables, facility operation constraints are treated as continuous variables, and the timetable in this assessment is updated hourly. This hourly update is used only in the scheme-level engineering assessment and should be distinguished from the 15-min rolling control interval used in the closed-loop validation experiments.

Based on the engineering model defined by Tables 7–11, two operation schemes were compared.

Scheme 1: Energy consumption under the existing operation strategy.

Scheme 2: Energy consumption under an optimized operation scheme generated using the proposed EM-enhanced heuristic optimization procedure within the engineering pre-evaluation setting.

This scheme-level optimization is separate from the eighteen-scenario closed-loop algorithm comparison reported above. Table 12 lists the detailed operational parameters of the two schemes, where the parameters of Scheme 2 were obtained through iterative optimization using the proposed method.

As shown in Table 13, under the specified enterprise-provided assumptions, total energy consumption decreases from 5860 GJ in Scheme 1 to 5220 GJ in Scheme 2, corresponding to an estimated energy-saving potential of approximately 10.92%.

Using the conversion factor of 1 GJ = 277.78 kWh and the local equivalent

Table 11. Operational parameters of the two scheduling schemes.

Equipment	**Unit**	**Scheme 1**				**Scheme 2**			
		1	2	3	4	1	2	3	4
Heating equipment	Supply flow (m^3/s)	6	5	6	12	5	5	5	10
Cooling equipment	Supply flow (m^3/s)	6	12	6	5	5	11.2	7.3	6
Ventilation equipment	Ventilation rate (m^3/s)	3	2	3	5	3	2.6	4	5
Air exchange equipment	Intake flow (m^3/s)	17	10	10	15	19	10	11	17
Ventilation system	Start time	07:00	07:00	07:00	07:00	06:00	06:00	04:00	06:00
Ventilation system	End time	22:00	22:00	22:00	22:00	22:00	22:00	22:00	22:00

Table 12. Comparison of the two scheduling schemes.

Energy component	**Scheme 1**	**Scheme 2**
Heating equipment (GJ)	3460	2130
Cooling equipment (GJ)	1220	1190
Electrical equipment (GJ)	1180	1900
Total energy use (GJ)	5860	5220
Relative total energy use	1	0.891
Change relative to Scheme 1	0%	-10.92%

electricity price of 0.91 RMB/kWh adopted by the enterprise, the economic comparison for the accounting period considered by the enterprise is summarized as follows:

- The total energy cost of Scheme 1 is approximately 1,481,278 RMB.
- The total energy cost of Scheme 2 is approximately 1,319,500 RMB.
- Compared with Scheme 1, Scheme 2 yields an estimated energy-cost saving of approximately 161,778 RMB for the accounting period considered by the enterprise.

Under the specified enterprise-provided assumptions, the optimized scheduling scheme reduces total energy consumption by 10.92% and corresponds to an estimated energy-cost saving of 161,778 RMB for the accounting period considered by the enterprise. Under the specified engineering assumptions, the case study supports the use of the CPES optimization framework for scheme comparison, control pre-evaluation, and safety-oriented operational verification before field deployment.

6. Conclusions

This paper addresses rolling temperature–humidity control for industrial sericulture workshops under coupled weather, electricity-price, and process-load disturbances. Within a CPES and EnergyPlus co-simulation framework, this study formulates a discrete-time optimization model with a 15-min control interval and combines it with an EM-based rolling local-refinement strategy for baseline heuristic controllers.

Across eighteen formal evaluation scenarios, the EM-enhanced methods reduce the average composite objective values by 31.04%–59.56% relative to the corresponding baselines. Among the ten main baseline and EM-enhanced methods, EM-PSO achieved the lowest average composite objective value, 514.94, together with a comfort satisfaction rate of 1.0000. The improvement mainly results from reduced comfort-boundary penalties, with some trade-offs in energy cost and switching frequency.

The ablation study identifies priority-based critical-step selection as the dominant source of improvement. It also shows that the complete EM framework is not uniformly superior to all PSO-derived variants in the ablation

set, so the ablation results do not indicate additive synergy of all EM components. The main methodological contribution is therefore a transferable refinement layer that improves the baseline solvers in the paired ten-method comparison. The Wilcoxon signed-rank tests further indicate that EM-PSO significantly outperformed TS, SA, GA, and standard PSO within the current scenario set.

The industry-parameter-based case study yields a 10.92% reduction in total energy consumption under the specified operating assumptions. This estimate comes from a separate engineering pre-evaluation and is distinct from the eighteen-scenario closed-loop validation. Overall, the present findings are obtained in a simulation-based setting built on enterprise-provided parameters, public disturbance data, and surrogate-assisted prediction. Future work should extend the scenario set, incorporate field monitoring data, and examine long-term closed-loop operation in real workshops.

References

[1] M. Grieves, Digital twin: manufacturing excellence through virtual factory replication, White paper 1 (2014) (2014) 1–7.

[2] J. Zhang, T. Deng, H. Jiang, H. Chen, S. Qin, G. Ding, Bi-level dynamic scheduling architecture based on service unit digital twin agents, Journal of Manufacturing Systems 60 (2021) 59–79.

[3] G. Zhang, C. Huo, L. Zheng, X. Li, An architecture based on digital twins for smart power distribution system, in: 2020 3rd international conference on artificial intelligence and big data (ICAIBD), IEEE, 2020, pp. 29–33.

[4] H. Jiang, S. Qin, J. Fu, J. Zhang, G. Ding, How to model and implement connections between physical and virtual models for digital twin application, Journal of Manufacturing Systems 58 (2021) 36–51.

[5] H. Rahman, U. M. Shah, S. M. Riaz, K. Kifayat, S. A. Moqurrab, J. Yoo, Digital twin framework for smart greenhouse management using next-gen mobile networks and machine learning, Future Generation Computer Systems 156 (2024) 285–300.

[6] C. Guo, H. Yan, C. Chen, X. Li, H. Yang, Y. Yan, Automatic code generation method for building a co-simulation platform integrating building

automatic systems and EnergyPlus, Energy and Buildings 351 (2026) 116667.

[7] J. L. Svensen, X. Cheng, S. Boersma, C. Sun, Chance-constrained stochastic mpc of greenhouse production systems with parametric uncertainty, Computers and Electronics in Agriculture 217 (2024) 108578.

[8] P. Gao, M. Lu, H. Li, H. Mao, J. Hu, H. Wu, Greenhouse environmental control target constrained by discrete surface curvature and multi-objective optimization algorithm, Computers and Electronics in Agriculture 215 (2023) 108431.

[9] X. Li, L. Zhang, X. Wang, B. Liang, Forecasting greenhouse air and soil temperatures: A multi-step time series approach employing attention-based lstm network, Computers and Electronics in Agriculture 217 (2024) 108602.

[10] E. N. Pergantis, P. Dhillon, L. D. R. Premer, A. H. Lee, D. Ziviani, K. J. Kircher, Humidity-aware model predictive control for residential air conditioning: A field study, Building and Environment 266 (2024) 112093.

[11] S. Yang, W. Chen, M. P. Wan, A machine-learning-based event-triggered model predictive control for building energy management, Building and Environment 233 (2023) 110101.

[12] C. Tsolkas, E. Spiliotis, E. Sarmas, V. Marinakis, H. Doukas, Dynamic energy management with thermal comfort forecasting, Building and Environment 237 (2023) 110341.

[13] P. Hua, H. Wang, Z. Xie, R. Lahdelma, Multi-criteria evaluation of novel multi-objective model predictive control method for indoor thermal comfort, Energy 289 (2024) 129883.

[14] B. Schleich, N. Anwer, L. Mathieu, S. Wartzack, Shaping the digital twin for design and production engineering, CIRP annals 66 (1) (2017) 141–144.

[15] T. H.-J. Uhlemann, C. Lehmann, R. Steinhilper, The digital twin: Realizing the cyber-physical production system for industry 4.0, Procedia Cirp 61 (2017) 335–340.

[16] F. Biesinger, D. Meike, B. Kraß, M. Weyrich, A digital twin for production planning based on cyber-physical systems: A case study for a cyber-physical system-based creation of a digital twin, Procedia CIRP 79 (2019) 355–360.

[17] M. Groshev, C. Guimarães, J. Martín-Pérez, A. de la Oliva, Toward intelligent cyber-physical systems: Digital twin meets artificial intelligence, IEEE Communications Magazine 59 (8) (2021) 14–20.

[18] A. Saad, S. Faddel, O. Mohammed, Iot-based digital twin for energy cyber-physical systems: design and implementation, Energies 13 (18) (2020) 4762.

[19] K. M. Alam, A. El Saddik, C2ps: A digital twin architecture reference model for the cloud-based cyber-physical systems, IEEE access 5 (2017) 2050–2062.

[20] F. Rodríguez, M. Berenguel, F. García-Mañas, J. L. Guzmán, J. A. Sánchez-Molina, A multilayer control architecture for greenhouse crop production in agro-industrial districts: Conceptual framework, prospects and challenges, Smart Agricultural Technology 9 (2024) 100657.

[21] A. Costantino, A. L. Ghiberti, C. Bibbiani, A. Barbaresi, E. Fabrizio, Advancing digital twin development for controlled-environment agriculture: Comparative evaluation of two greenhouse energy models and their readiness for digital twin implementation, Smart Agricultural Technology 14 (2026) 102009.

[22] H. Kong, Z. Li, Z. Yu, J. Zhang, H. Wang, J. Wang, D. Gao, Environmental and economic multi-objective optimization of comprehensive energy industry: A case study, Energy 237 (2021) 121534.

[23] D. Huang, C. D. Dinga, Y. Tao, Z. Wen, Y. Wang, Multi-objective optimization of energy conservation and emission reduction in china's iron and steel industry based on dimensionality reduction, Journal of Cleaner Production 368 (2022) 133131.

[24] F. Matsunaga, V. Zytkowski, P. Valle, F. Deschamps, Optimization of energy efficiency in smart manufacturing through the application of

cyber–physical systems and industry 4.0 technologies, Journal of Energy Resources Technology 144 (10) (2022) 102104.

[25] R. Wang, L. Jiang, Y. Wang, A. P. Roskilly, Energy saving technologies and mass-thermal network optimization for decarbonized iron and steel industry: A review, Journal of Cleaner Production 274 (2020) 122997.

[26] M. Karmellos, G. Mavrotas, Multi-objective optimization and comparison framework for the design of distributed energy systems, Energy Conversion and Management 180 (2019) 473–495.

[27] A. Du, Y. Chen, D. Zhang, Y. Han, Multi-objective energy management strategy based on pso optimization for power-split hybrid electric vehicles, Energies 14 (9) (2021) 2438.

[28] C. Bua, Y. Wang, M. O. Ojo, S. Giordano, A. Zahid, Digital twin-enabled multi-zone adaptive lighting control in greenhouses using reinforcement learning optimization, Smart Agricultural Technology 14 (2026) 101984.

[29] A. Tryhuba, T. Hutsol, J. Česna, I. Tryhuba, K. Mudryk, S. Francik, S. Kukharets, I. Mishchenko, R. Oliinyk, Optimizing energy systems of livestock farms with computational intelligence for achieving energy autonomy, Scientific Reports 15 (1) (2025) Article 10777.

[30] D.-C. Wu, M. Momeni, A. Razban, J. Chen, Optimizing demand-controlled ventilation with thermal comfort and co2 concentrations using long short-term memory and genetic algorithm, Building and Environment 243 (2023) 110676.

[31] H. Mokhtari, A. Hasani, An energy-efficient multi-objective optimization for flexible job-shop scheduling problem, Computers & Chemical Engineering 104 (2017) 339–352.

[32] D. Wang, Y. Chen, W. Wang, C. Gao, Z. Wang, Field test of model predictive control in residential buildings for utility cost savings, Energy and Buildings 288 (2023) 113026.

[33] S. Kirkpatrick, C. D. Gelatt, M. P. Vecchi, Optimization by simulated annealing, Science 220 (4598) (1983) 671–680.

[34] F. Glover, Tabu search–part i, ORSA Journal on Computing 1 (3) (1989) 190–206.

[35] C. D. Iweh, E. R. Akupan, Control and optimization of a hybrid solar pv–hydro power system for off-grid applications using particle swarm optimization (pso) and differential evolution (de), Energy Reports 10 (2023) 4253–4270.

[36] F. Glover, Tabu search–part ii, ORSA Journal on Computing 2 (1) (1990) 4–32.

[37] M. Kumar, S. C. Sharma, Pso-cogent: Cost and energy efficient scheduling in cloud environment with deadline constraint, Sustainable Computing: Informatics and Systems 19 (2018) 147–164.

[38] A. Maria, Introduction to modeling and simulation, in: Proceedings of the 29th conference on Winter simulation, 1997, pp. 7–13.

[39] P. K. Davis, Distributed interactive simulation in the evolution of dod warfare modeling and simulation, Proceedings of the IEEE 83 (8) (1995) 1138–1155.

[40] D. R. Russell, W. K. McQuay, The joint modeling and simulation system: a common modeling architecture for the dod, in: Proceedings of the 25th conference on Winter simulation, 1993, pp. 984–988.

[41] J. W. Hollenbach, W. L. Alexander, Executing the dod modeling and simulation strategy—making simulation systems of systems a reality, in: Proceedings of the 29th conference on Winter simulation, 1997, pp. 948–954.

[42] O. Balci, Verification, validation, and accreditation, in: 1998 winter simulation conference. proceedings (cat. no. 98ch36274), Vol. 1, IEEE, 1998, pp. 41–48.

[43] IEEE Computer Society, IEEE Recommended Practice for Verification, Validation and Acceptance/Accreditation of a Distributed Simulation: An Overlay to the Distributed Simulation Engineering and Execution Process, Standard IEEE Std 1730.2-2022, IEEE, New York (2022).

[44] Simulation Interoperability Standards Organization, Guide for Generic Methodology for Verification and Validation (GMVV) to Support Acceptance of Models, Simulations, and Data, GM-VV Volume 2: Implementation Guide, Guide SISO-GUIDE-001.2-2013, Simulation Interoperability Standards Organization, Orlando (2013).